

*Supplemental Information for*

## **Siderophore-Promoted Dissolution of Chromium from Hydroxide Minerals**

by

Owen W. Duckworth,<sup>1,\*</sup> Martin M. Akafia,<sup>1</sup> Megan Y. Andrews,<sup>1</sup>  
and John R. Bargar<sup>2</sup>

Six Figures, One Table

*Fitting extended X-ray absorption fine structure spectra to existing structural models of aqueous Cr(III)-siderophore complexes.*

To determine if the structures of the DFOB- and rhizoferrin-promoted dissolution products were consistent with those of aqueous Cr(III)-siderophore complexes, extended X-ray absorption fine structure (EXAFS) spectra were fit with a model containing a multiple scattering path based on previous models of aqueous siderophore complexes.<sup>1-3</sup> Amplitude and phase functions were calculated using FEFF 6 from the crystallographic model of solid ferrioxamine E,<sup>4</sup> with Cr replacing Fe as the central atom. The amplitude reduction factor ( $S_0^2$ ) was fixed at 0.86.<sup>3</sup> The first shell represents the oxygen atoms in chromium's first coordination sphere. For this shell, coordination number ( $N$ ) was allowed to float freely. The second shell represents the carbon and nitrogen atoms contained in the hydroxamate and carboxylate moieties, and was modeled as a single shell of six carbon atoms. A third shell, modeled as 6 carbon atoms, represents the average position of the proximal atoms in the siderophore backbone. A triangular three-legged multiple scattering shell containing 12 metal-carbon/nitrogen-oxygen paths was also utilized to facilitate comparison to recently determined metal-siderophore complex structures.<sup>1-3</sup> For Cr(III)(H<sub>2</sub>O)<sub>6</sub><sup>3+</sup>, only the first shell was used in the fit; for rhizoferrin, an additional shell containing 2 oxygen atoms was utilized to model the contribution of distal oxygen atoms in the carboxylate groups.<sup>1, 2</sup> The Debye-Waller disorder parameter ( $\sigma^2$ ) and the interatomic distance ( $R$ ) for each shell were floated freely during optimization whereas  $\Delta E_0$  was fit as a common value for all shells but was allowed to float during optimization.

Modeling of XAS spectra was conducted to determine if the structure of dissolution products was consistent with those of metal-siderophore complexes (Figure 5). To that end, we utilized a fitting motif that previously has been used to fit Fe(III) and Mn(III) complexes with

DFOB and rhizoferrin.<sup>2</sup> In addition to the first shell oxygen atoms at  $R + \Delta R \approx 1.5 \text{ \AA}$ , we specifically fit the FT feature at  $R + \Delta R \approx 2.1 \text{ \AA}$  with 6 carbon atoms and 12 multiple scattering paths corresponding to contributions from atoms in carboxylate or hydroxamate groups. Six proximal carbon atoms (at  $R_C = 4.26\text{--}4.35 \text{ \AA}$ ) in the siderophore backbone correspond to the FT peak at  $R + \Delta R = 3.8 \text{ \AA}$ . Additionally, 2 oxygen atoms are included to fit distal oxygen atoms associated with carboxylate moieties in the Cr(III)-rhizoferrin complex (corresponding to the  $R + \Delta R = 2.8 \text{ \AA}$  FT peak). The fit for the DFOB-promoted dissolution product agree well with those of a dissolved Cr(III)HDFOB<sup>+</sup> complex,<sup>3</sup> and the determined interatomic distances are generally consistent with previous results with metal-DFOB<sup>5-7</sup> and metal-rhizoferrin<sup>1, 2</sup> complexes, further suggesting that the Cr(III)-siderophore complexes are the dominant dissolved Cr species at alkaline pH.

The quality of the data fits is consistent with previous efforts to model metal-siderophore structures.<sup>1-3, 5-11</sup> However, inspection of the Fourier Transform data reveals that the fits could be improved in the region between  $R + \Delta R = 2.0\text{--}3.8 \text{ \AA}$ , where the fits underpredict the amplitude of specific features. Multiple scattering effects, which are highly dependent on geometric configuration of the complex,<sup>12, 13</sup> contribute significantly to spectral features in this region.<sup>2, 8, 10</sup> It is possible that the simplified model we are using to simulate multiple scattering effects (the crystallographic coordinates for solid ferrioxamine E<sup>4</sup> with Cr substituted for Fe) does not adequately recreate these features. Additionally, the  $\sigma^2$  values associated with the shells containing the carbon backbone (3<sup>rd</sup> shell carbons), distal carboxylate oxygen atoms, and multiple scattering features have large errors (greater than the parameter value), indicating that the fit parameters poorly constrain this feature. The shortcomings may indicate that our model misses some nuanced aspects of the structures of these Cr(III)-siderophore complexes. It is

known that Cr(III)-siderophore complexes may preferentially form multiple stereoisomers,<sup>14, 15</sup> which may have a distinct geometry from the iron complex used as the geometric basis of our simulation. Our results thus should be viewed as approximations of the structures of the Cr(III)-siderophore complexes, which may contain significant configurational features that are not captured by our models. Although we do not anticipate that the prevalence of specific isomers will have a significant effect on the solution or geochemical behavior of metal-siderophore complexes, it has been shown that different isomers may interact differently with cellular uptake systems.<sup>14, 16-18</sup> Because the stereochemical configuration potentially affects the bioavailability of Cr(III)-siderophore complexes and the entry of Cr into the food web of ecosystems, more study is needed to better understand the isomeric composition of dissolution products.

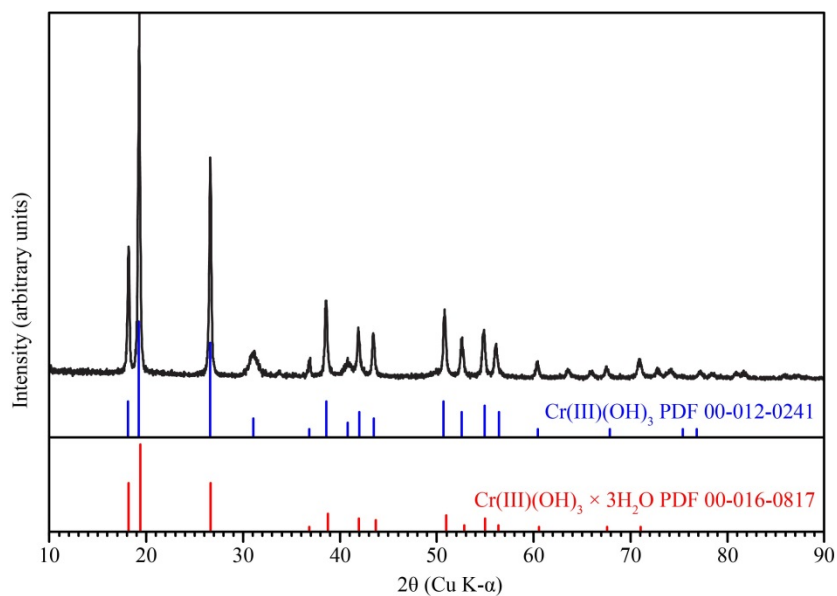
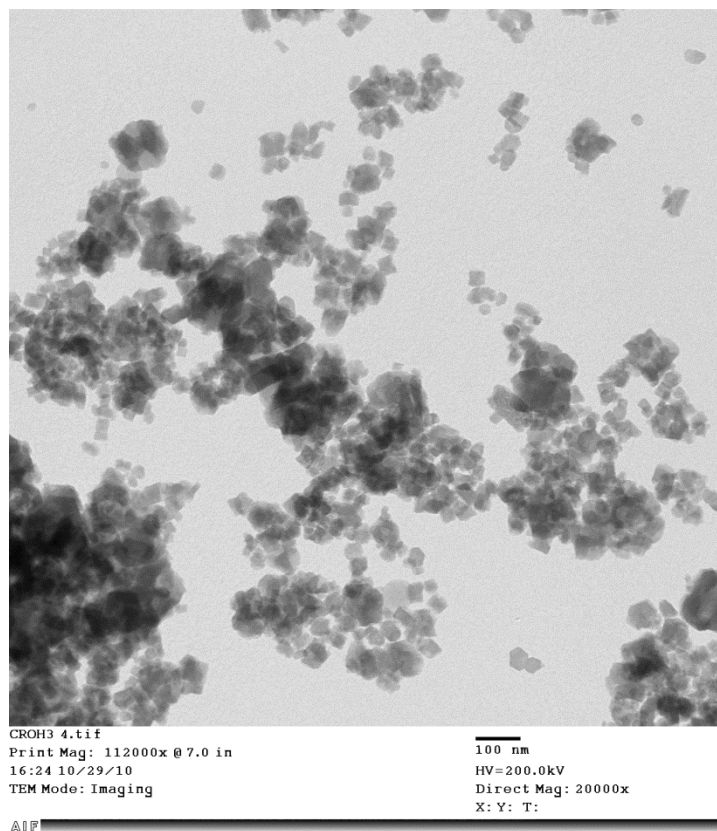


**Figure ESI1.** Transmission electron micrograph and X-ray diffractogram of  $\text{Cr(III)(OH)}_3$ . Numbers of reference diffraction patterns are the International Centre for Diffraction Data card numbers.<sup>19</sup>

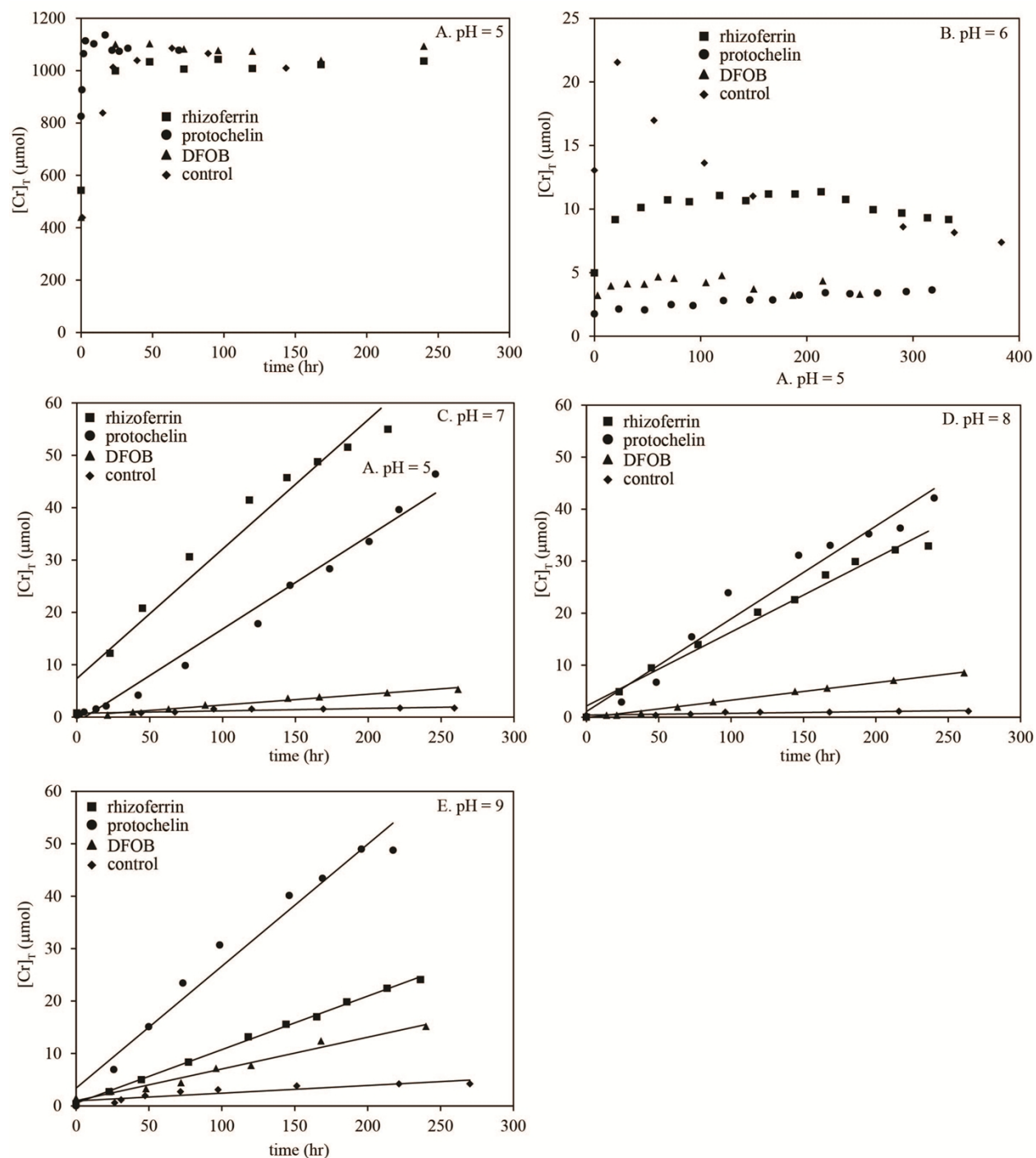


**Figure ES12.** Example plots showing the dissolution of  $Cr(III)(OH)_3$  in the presence of different siderophores at (A) pH = 5, (B) pH = 6, (C) pH = 7, (D) pH = 8, (E) pH = 9. Lines represent least square fits to the time course data. Conditions:  $0.2 \text{ g L}^{-1} Cr(III)(OH)_3$ ,  $0.1 \text{ M NaCl}$ ,  $10 \text{ mM}$  buffer,  $25^\circ\text{C}$ ,  $100 \text{ mM}$  DFOB (triangles),  $100 \text{ }\mu\text{M}$  rhizoferrin (squares),  $100 \text{ }\mu\text{M}$  protochelin (circles), no siderophore (diamonds).

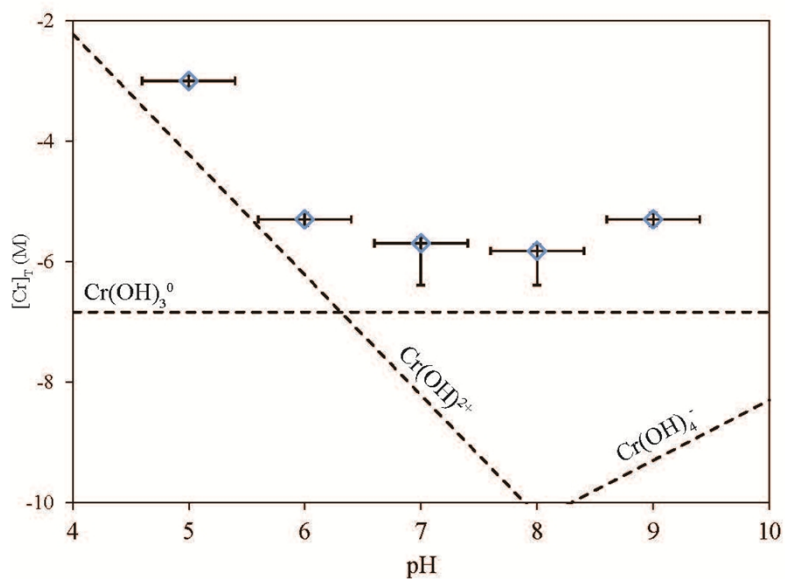


**Figure ESI3.** Solubility diagram for Cr(III)(OH)<sub>3</sub>. Dashed lines are the calculated solubilities of specific Cr(III) species whereas open points are measured  $[Cr]_T$  values from control experiments. Points at pH =7-8 are above the limit of detection but below the limit of quantitation, indicating they are within the range of vertical error bars. Thermodynamic data used to generate solubility lines are from Rai et al.<sup>20</sup>

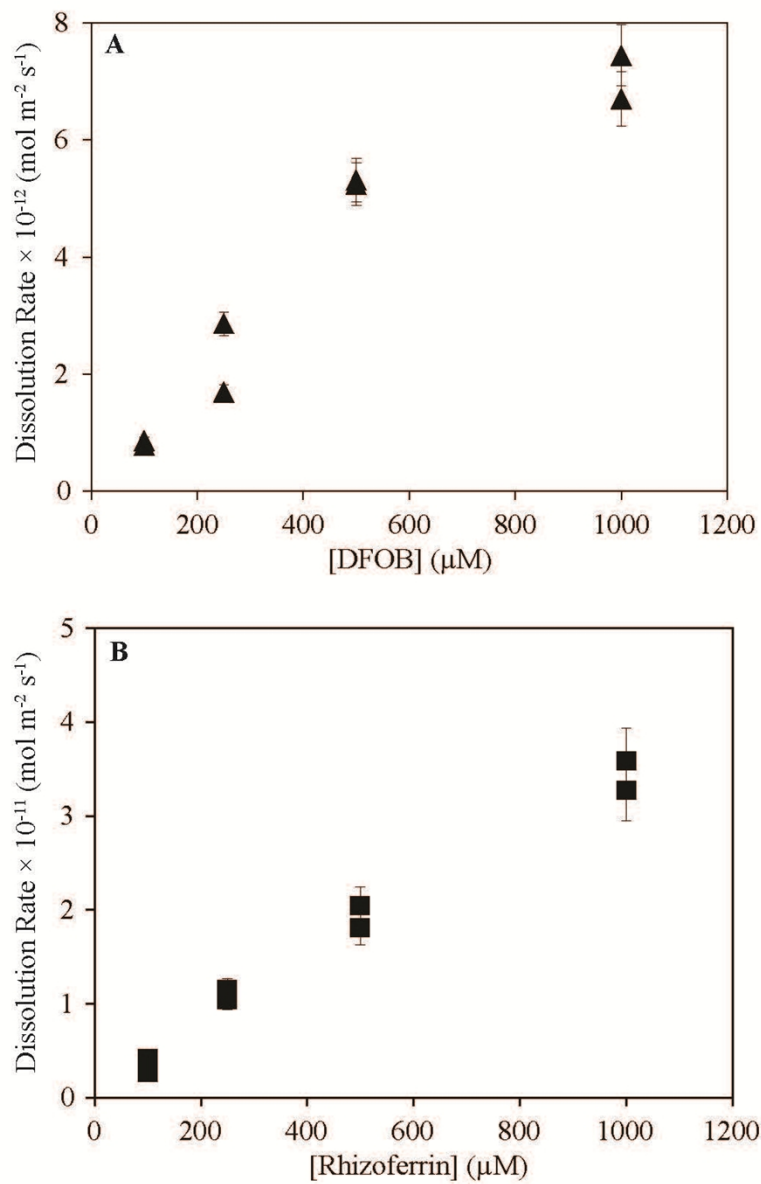


**Figure ESI4.** Dissolution rates for Cr(III)(OH)<sub>3</sub> plotted as a function of siderophore concentration in the presence of (A) DFOB and (B) rhizoferrin. Conditions: pH = 8, 0.2 g L<sup>-1</sup> Cr(III)(OH)<sub>3</sub>, 0.1 M NaCl, 10 mM buffer, 25°C.

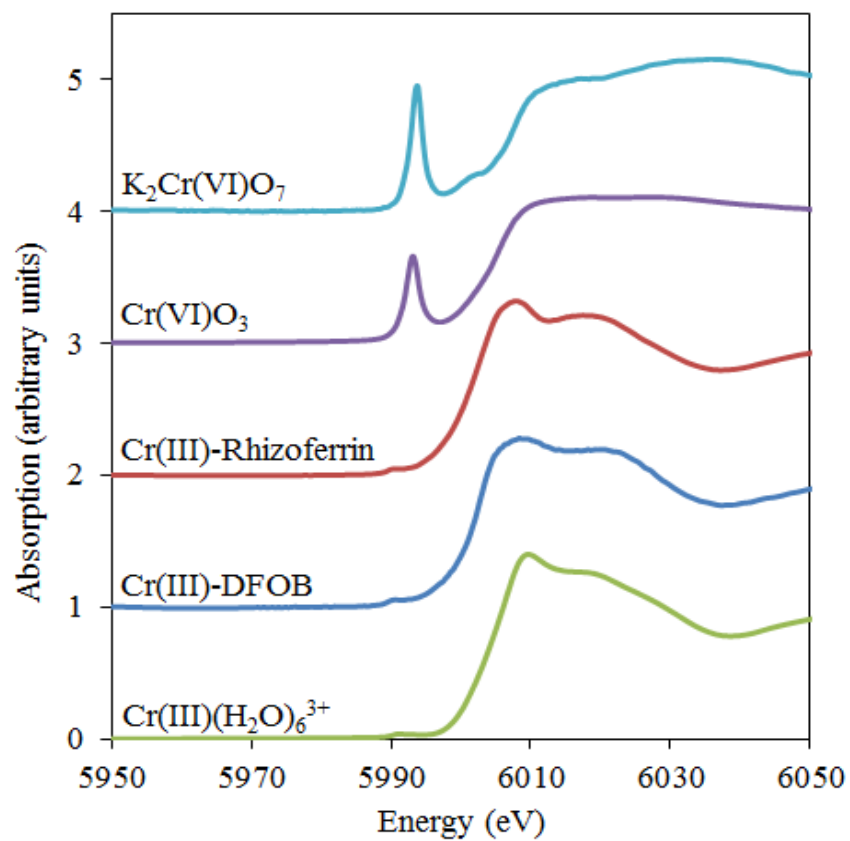


**Figure ESI5.** Cr K  $\alpha$ -edge XANES spectra of the products of Cr(III)(OH)<sub>3</sub> dissolution in the presence of (A) rhizoferrin and (B) DFOB. Also included is a Cr(III)(H<sub>2</sub>O)<sub>6</sub><sup>3+</sup> reference spectrum (C).<sup>21</sup>

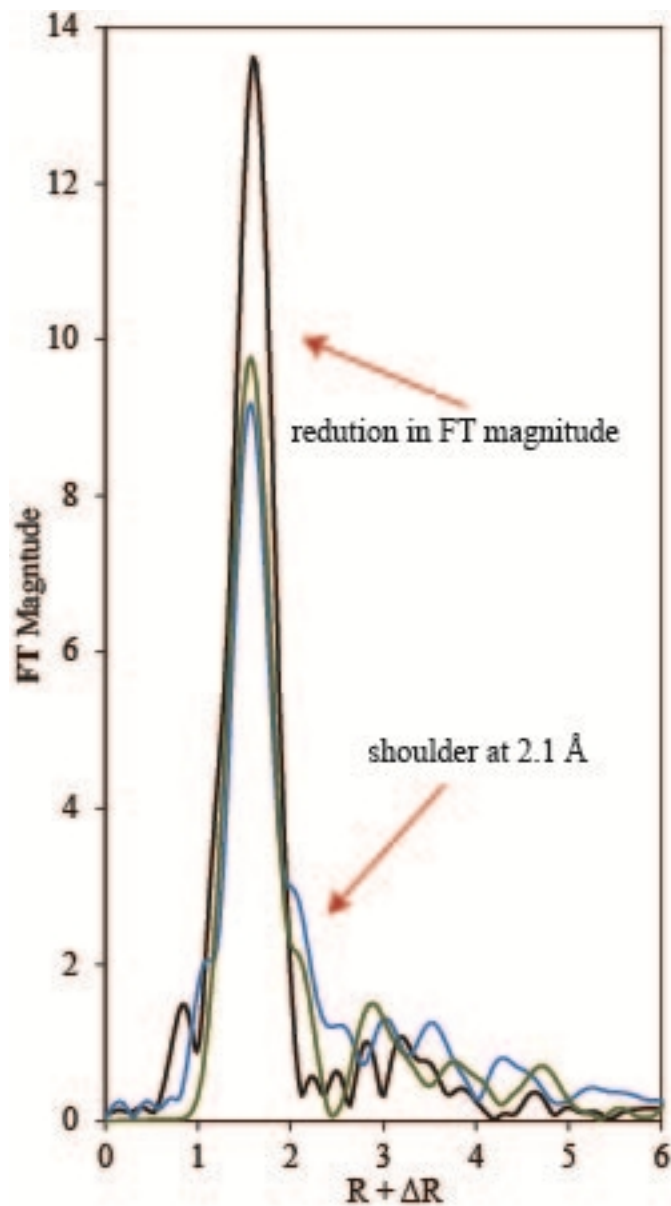


**Figure ESI6.** Expanded plot showing the superimposed FT magnitudes of Cr K  $\alpha$ -edge EXAFS spectra for Cr(III)(OH)<sub>3</sub> (black) and dissolution products in the presence of DFOB (blue) and (A) rhizoferrin (green).

**Table ES11.** Coordination numbers ( $N$ ), interatomic distances ( $R$ ; Å), and Debye-Waller factors ( $\sigma^2$ ; Å<sup>2</sup>) for Cr(III)-siderophore complexes derived from dissolution of Cr(III)(OH)<sub>3</sub>. For all fits, amplitude reduction factors ( $S_0^2$ ) were set at 0.86.<sup>3</sup> Numbers in brackets are experimental uncertainties in the last decimal place. Spectra of a synthetic Cr(III)HDFOB<sup>+</sup> complex<sup>3</sup> and Cr(III)(H<sub>2</sub>O)<sub>6</sub><sup>3+</sup> are included for comparison. <sup>s</sup>Fixed coordination number. N.A. indicates parameters are not applicable to the model.

species	First Shell Cr–O			Second Shell Cr–C/N			Third Shell Cr–C			Carboxyl Cr–O			Multiple Cr–C/N–O		
	N	R (Å)	$\sigma^2$	N	R (Å)	$\sigma^2$	N	R (Å)	$\sigma^2$	N	R (Å)	$\sigma^2$	N	R (Å)	$\sigma^2$
Cr(III)-rhizoferrin	5.6[9]	1.988[9]	0.004[1]	6	2.86[8]	0.02[1]	6	4.36[5]	0.004[5]	2	3.26[5]	0.003[5]	12	2.88[5]	0.002[4]
Cr(III)-DFOB	4.9[8]	1.984[9]	0.004[1]	6	2.82[3]	0.009[3]	6	4.29[8]	0.008[9]		N.A.		12	3.0[2]	0.02[3]
Cr(III)HDFOB <sup>+</sup> <sup>3</sup>	7[1]	1.94[1]	0.005[1]	6	2.85[2]	0.003[2]	25	4.24[3]	0.009[3]		N.A.			N.A.	
Cr(III)(H <sub>2</sub> O) <sub>6</sub> <sup>3+</sup>	6.7[4]	1.975[3]	0.002[4]		N.A.			N.A.			N.A.			N.A.	

## References.

1. M. M. Akafia, J. M. Harrington and O. W. Duckworth, *Geochim. Cosmochim. Acta*, 201X, submitted.
2. J. M. Harrington, D. L. Parker, J. R. Bargar, A. A. Jarzecki, B. M. Tebo, G. Sposito and O. W. Duckworth, *Geochim. Cosmochim. Acta*, 2012, **88**, 106-119.
3. B. I. Kruft, J. M. Harrington, O. W. Duckworth and A. A. Jarzecki, *J. Biol. Inorg. Chem.*, 2013, **129**, 150-161.
4. M. B. Hossain, M. A. F. Jalal, D. van der Helm, K. Shimizu and M. Akiyama, *J Chem Crystallogr*, 1998, **28**, 53-56.
5. O. W. Duckworth, J. R. Bargar and G. Sposito, *Geochim. Cosmochim. Acta*, 2008, **72**, 3371-3380.
6. O. W. Duckworth, J. R. Bargar and G. Sposito, *Environ. Sci. Technol.*, 2009, **43**, 343–349.
7. O. W. Duckworth, A. A. Jarzecki, J. R. Bargar, O. Oyerinde, T. G. Spiro and G. Sposito, *Marine Chem.*, 2009, **113**, 114–122.
8. J. M. Harrington, J. M. Bargar, A. A. Jarzecki, L. A. Sombers, J. G. Roberts and O. W. Duckworth, *BioMetals*, 2012, **25**, 393-412.
9. D. C. Edwards and S. C. B. Myneni, *J. Phys. Chem. A*, 2005, **109**, 10249-10256.
10. T. Karlsson and P. Persson, *Geochim. Cosmochim. Acta*, 2010, **74**, 30-40.
11. B. Mishra, E. A. Haack, P. A. Maurice and B. A. Bunker, *Environ. Sci. Technol.*, 2009, **43**, 94-100.
12. S. M. Webb, B. M. Tebo and J. R. Bargar, *Am. Min.*, 2005, **90**, 1342-1357.
13. E. A. Hudson, P. G. Allen, L. J. Terminello, M. A. Denecke and T. Reich, *Physical Review B*, 1996, **54**, 156-165.
14. C. J. Carrano, H. Drechsel, D. Kaiser, G. Jung, B. Matzanke, G. Winkelmann, N. Rochel and A. M. Albrecht-Gary, *Inorg. Chem.*, 1996, **35**, 6429-6436.
15. J. Leong and K. N. Raymond, *J. Am. Chem. Soc.*, 1975, **97**, 293-296.
16. T. D. Y. Chung, B. F. Matzanke, G. Winkelmann and K. N. Raymond, *J. Bacteriol.*, 1986, **165**, 283-287.
17. C. J. Carrano, A. Thieken and G. Winkelmann, *BioMetals*, 1996, **9**, 185-189.
18. G. Müller, Y. Isowa and K. N. Raymond, *J Biol Chem*, 1985, **260**, 13921-13926.
19. ICDD, ed. S. Kabekkodu, International Centre for Diffraction Data), Newtown Square, PA, Editon edn., 2010, vol. Set 60.
20. D. Rai, B. M. Sass and D. A. Moore, *Inorg. Chem.*, 1987, **26**, 345-349.
21. J. Bang, North Carolina State University, 2002.